Published in final edited form as:
Neuron. 2010 January 14; 65(1): 53–65. doi:10.1016/j.neuron.2009.12.007.

Deslivery of $GABA_A$Rs to synapses is mediated by HAP1-KIF5 and disrupted by mutant huntingtin

Alison E. Twelvetrees[1], **Eunice Y. Yuen**[2], **I. Lorena Arancibia-Carcamo**[1], **Andrew F. MacAskill**[1], **Philippe Rostaing**[3], **Michael J. Lumb**[1], **Sandrine Humbert**[4], **Antoine Triller**[3], **Frederic Saudou**[4], **Zhen Yan**[2], and **Josef T. Kittler**[1]

[1]Department of Neuroscience, Physiology and Pharmacology, University College London, Gower Street, London, WC1E 6BT, UK

[2]Department of Physiology and Biophysics, State University of New York at Buffalo, Buffalo, New York 14214, USA

[3]INSERM U789, Biologie Cellulaire de la Synapse N&P, Ecole Normale Superieure Paris, 46 Rue d'Ulm 75005 Paris, France

[4]Unite Mixte de Recherche 146, Centre National de la Recherche Scientifique, Institut Curie, Building 110, Centre Universitaire, 91405, Orsay Cedex, France

Abstract

The density of $GABA_A$ receptors ($GABA_A$Rs) at synapses regulates brain excitability, and altered inhibition may contribute to Huntington's disease, which is caused by a polyglutamine repeat in the protein huntingtin. However, the machinery that delivers $GABA_A$Rs to synapses is unknown. We demonstrate that $GABA_A$Rs are trafficked to synapses by the kinesin family motor protein 5 (KIF5). We identify the adaptor linking the receptors to KIF5 as the huntingtin associated protein 1 (HAP1). Disrupting the HAP1-KIF5 complex decreases synaptic $GABA_A$R number, and reduces the amplitude of inhibitory postsynaptic currents. When huntingtin is mutated as in Huntington's disease, $GABA_A$R transport and inhibitory synaptic currents are reduced. Thus, HAP1-KIF5 dependent $GABA_A$R trafficking is a fundamental mechanism controlling the strength of synaptic inhibition in the brain. Its disruption by mutant huntingtin may explain some of the defects in brain information processing occurring in Huntington's disease, and provides a new molecular target for therapeutic approaches.

Synaptic inhibition plays a critical role in regulating neuronal excitability and information processing in the brain. The number of $GABA_A$Rs expressed in the surface membrane and at synaptic sites is a critical determinant of inhibitory synapse strength (Arancibia-Carcamo and Kittler, 2009; Jacob et al., 2008), but the molecular machinary that deliver $GABA_A$Rs to synapses remain unclear. Importantly, the role of kinesin family (KIF) microtubule motors in regulating the strength and plasticity of GABAergic transmission is unknown, as is the identity of the adaptor molecules which link $GABA_A$Rs to their trafficking motors.

Correspondence should be addressed to Dr Josef Kittler (j.kittler@ucl.ac.uk).

Alterations in protein trafficking to neuronal membranes, including altered trafficking of $GABA_A$Rs, occur in a number of neurological and psychiatric diseases (Jacob et al., 2008; Olkkonen and Ikonen, 2006). Altered $GABA_A$R trafficking may underlie or exacerbate disease progression by altering the excitatory/inhibitory balance, leading to neuronal excitotoxicity and/or disrupted information processing (Arancibia-Carcamo and Kittler, 2009; Jacob et al., 2008). In Huntington's disease (HD), a polyglutamine expansion in the huntingtin protein (polyQ-htt) results in cell death and neurodegeneration of specific neuronal populations, leading to uncontrolled movements, personality changes, dementia and eventually death within 10–20 years of the first symptoms. In addition to roles in regulating apoptosis and transcription, huntingtin may have a neurotoxic role in HD by altering intracellular transport of proteins, including transport of NMDA receptors (Fan and Raymond, 2007; Gunawardena et al., 2003; Smith et al., 2005; Szebenyi et al., 2003). Whether mutant huntingtin disrupts $GABA_A$R trafficking, leading to compromised inhibition and disruption of the excitatory/inhibitory balance, remains unknown.

A key mediator of pathological alterations in protein trafficking produced by polyQ-htt is the huntingtin associated protein 1 (HAP1; (Gauthier et al., 2004; Li and Li, 2005; Li et al., 1995). HAP1 interacts directly with $GABA_A$Rs and facilitates their recycling back to synapses after they have been internalized from the surface membrane, and so can regulate the strength of inhibitory synaptic transmission (Kittler et al., 2004), but how HAP1 regulates $GABA_A$R trafficking to synapses and whether this trafficking is a target for mutant polyQ-htt remains unknown.

Here, using biochemical, imaging and electrophysiological approaches, we show that HAP1 is an adaptor which links $GABA_A$Rs to KIF5 motors, forming a motor protein complex for rapid delivery of $GABA_A$Rs to synapses. Furthermore, mutant huntingtin containing a polyQ expansion which disrupts HAP1 function (Gauthier et al., 2004; Li et al., 1995) inhibits this KIF5-dependent $GABA_A$R trafficking and synaptic delivery. Thus, KIF5-dependent transport is critical for delivery of $GABA_A$Rs to inhibitory synapses, and disruption of this complex by mutant huntingtin may lead to altered synaptic inhibition and increased neuronal excitability in Huntington's disease.

Results

The delivery of $GABA_A$Rs to synapses is mediated by the motor KIF5

The kinesin motor protein KIF5 is a critical determinant of intracellular transport processes in neurons (Hirokawa and Takemura, 2005). To investigate if KIF5 activity is important for inhibitory transmission, we carried out whole-cell patch clamp recordings to measure inhibitory synaptic transmission in cortical neurons dialyzed via the electrophysiological recording pipette with an antibody demonstrated to block KIF5 motor protein activity [kinesin function blocking antibody SUK4 (Ingold et al., 1988; Jaulin et al., 2007)], which does not inhibit myosin- or dynein-based motility (Bi et al., 1997; Lane and Allan, 1999). This was compared to neurons dialyzed with a control antibody (9E10) that does not recognize KIF5. Dialysis of SUK4 (Figure 1A, C&F) caused a rapid reduction in mIPSC amplitude within 20 min of recording (Figure 1F: SUK4, 36.2±3% reduction in mean mIPSC amplitude n = 7, $P < 0.05$), as can clearly be seen in representative mIPSC traces (Figure 1C) and by a leftward shift to smaller amplitudes in cumulative probability plots (Figure 1A). In contrast there was no significant decrease in mean mIPSC amplitude in control 9E10 dialyzed neurons (Figure 1D&F: 9E10, 5.6±1.7% reduction, n = 5). Neither SUK4 or 9E10 antibody were found to affect mIPSC interval (Figure 1B, E&F: SUK4, 8.2±4.4% reduction in mean mIPSC interval; 9E10, 5.3±1.6% reduction). Dialysis of SUK4 antibody did not affect mIPSC kinetics, implying that KIF5 does not selectively transport $GABA_A$Rs with particular kinetics (see Table S1). Similar

results were also seen with SUK4 and 9E10 FAb fragments (Figure S1A–E). Thus, our results support a key role for KIF5 function in maintaining inhibitory synaptic transmission.

We hypothesized that the effect of SUK4 on inhibitory transmission was mediated by blocking KIF5-dependent $GABA_AR$ delivery to synapses. To test this, SUK4 or control 9E10 antibody was introduced into cultured neurons by complexing with a membrane permeant carrier peptide (Coulpier et al., 2002; Morris et al., 2001) and the effect on surface $GABA_AR$ cluster area was determined using immunofluorescence and confocal laser scanning microscopy (CLSM). Cell surface synaptic $GABA_AR$ clusters were identified with an antibody to the extracellular domain of the $GABA_AR$ γ2 subunit while antibodies to the vesicular inhibitory amino acid transporter (VIAAT; a marker of inhibitory presynaptic terminals (Dumoulin et al., 1999)) were used to identify inhibitory synapses on neuronal dendrites. A mouse secondary antibody verified that SUK4 penetrated the neurons (see Figure S1G). Neurons treated with SUK4 showed a significant decrease in $GABA_AR$ cluster area in dendrites compared to control mock treated or 9E10 treated neurons (Figure 1G&H; SUK4 treatment reduced $GABA_AR$ cluster area by 46.5±11.9% compared to 9E10 controls, n = 5, $P < 0.01$), but with no change in the ratio of synaptic to non-synaptic $GABA_AR$ clusters (Figure S1F) strongly suggesting that blocking KIF5 activity decreases the delivery of $GABA_ARs$ to synapses.

We also compared the effect of blocking KIF5 activity on $GABA_AR$ responses with its effect on NMDA receptor (NMDAR) mediated responses, which are trafficked by a different KIF, the motor protein KIF17 (Guillaud et al., 2003; Setou et al., 2000). Compared to control inactive (boiled) SUK4 antibody (Figure 1I&K), SUK4 dialysis rapidly and dramatically reduced $GABA_AR$ mediated whole cell responses in recorded neurons (Figure 1I&K: 35.1±7.9% reduction in GABA response within 20 mins with SUK4, n = 6, $P < 0.05$, compared to 8.7 ±2.2% reduction for inactive boiled SUK4, n = 7) whereas neither active nor inactive SUK4 affected NMDAR mediated responses (Figure 1J&K: SUK4: 9.4±1.8% reduction in NMDA response, n = 7; boiled SUK4: 8.1±1.7%, n = 7), further supporting the specificity of KIF5 for selectively trafficking $GABA_ARs$ to synapses.

HAP1 is the adaptor linking KIF5 to $GABA_ARs$

If KIF5 is important for synaptic delivery of $GABA_ARs$, then we would expect to detect localisation of KIF5 and $GABA_ARs$ to the same neuronal compartments. In agreement with this, immunofluorescence and CLSM with antibodies to the $GABA_AR$ γ2 subunit and antibodies specific to KIF5B (Figure 2A) or KIF5C (Figure 2B), revealed that a proportion of KIF5 staining colocalized with $GABA_AR$ clusters in the neuronal somata and dendrites of cultured hippocampal and cortical neurons (see also Figure S2 for whole images of hippocampal neurons and for labeling of cortical neurons). Furthermore, electron microscopy of *in vivo* hippocampus and rat ventral spinal cord, revealed that KIF5-positive deposits were consistently found in the vicinity of postsynaptic membranes and decorating the postsynaptic side of symmetrical type 2 contacts, defined as inhibitory by the pleiomorphic nature of the vesicles within the presynaptic boutons and by their narrow (15–20 nm) synaptic cleft (Figures 2C–H). With pre-embedding immunolabelling and gold-toned silver intensified nanogold particles, KIF5 staining was found associated with small subsynaptic intracellular cisternae, which were often located below or at the edge of postsynaptic differentiations that may be part of subsynaptic tubulovesicular endosomes (Figures 2C&E). Double detection of GAD and KIF5, with immunoperoxidase and gold toned silver-intensified nanoparticles respectively, confirmed the inhibitory nature of the presynaptic terminals (Figure 2G&H).

We would also expect to detect protein complexes of KIF5 and $GABA_ARs$ *in vivo*. To investigate this we carried out glutathione-S-transferase (GST) pull downs and co-immunoprecipitation assays from rat brain lysate. GST-fusion proteins of the $GABA_AR$ β1-3 subunit intracellular domains (Figure 2I), or rat brain immunoprecipitated $GABA_ARs$ (Figure

2J) could readily co-precipitate KIF5 heavy chains, providing the first evidence that KIF5 motor proteins form complexes with $GABA_A$Rs *in vivo*. Motor proteins often determine cargo selectivity by linking to the cargo via an adaptor protein (Hirokawa and Takemura, 2005). HAP1 is involved in motor protein dependent transport of neuronal cargo, associating with motor protein complexes (Engelender et al., 1997; Gauthier et al., 2004; Li et al., 1998; McGuire et al., 2005), as well as interacting directly with $GABA_A$Rs (Kittler et al., 2004), and therefore was a good candidate adaptor to link $GABA_A$R transport vesicles with KIF5 motors. HAP1 immunoprecipitated from solubilized brain extracts readily co-precipitated KIF5, as demonstrated with either a pan anti-KIF5 antibody (which recognises all three KIF5 heavy chains, Figure 2K) or using anti-KIF5B and anti-KIF5C specific antibodies (Figure 2L&M, respectively). In the reverse experiment HAP1 readily co-precipitated with immunoprecipitated KIF5C or $GABA_A$R β3 subunits, further confirming that *in vivo* $GABA_A$Rs are found in complexes with HAP1 and KIF5 (Figure 2N). To test if the interaction between HAP1 and KIF5A–C heavy chains was direct, we performed GST fusion protein affinity purification experiments with GST-HAP1 and individual ^{35}S-methione-labeled KIF5A-C heavy chains or the light chain (KLC), which confirmed a direct interaction of KIF5 heavy chains with HAP1 (highest for KIF5B and KIF5C isoforms; Figure 2O&P). Thus HAP1 is the adaptor linking KIF5 to $GABA_A$Rs.

KIF5 mediates insertion of $GABA_A$Rs into the surface membrane at synapses

To further investigate the mechanism of KIF5-dependent $GABA_A$R trafficking we identified the molecular determinants of the HAP1-KIF5 interaction. KIF5 heavy chains comprise an N-terminal motor domain and a C-terminal non-motor domain. Initial experiments, using co-immunoprecipitation and co-expression of epitope tagged KIF5C N-terminal motor domain or C-terminal non-motor domain proteins, revealed that HAP1 interacts with the KIF5C non-motor domain (Figure S3) which comprises the stalk domain, the kinesin light chain binding domain and the cargo binding domain. Using additional GFP tagged constructs for KIF5B (or KIF5C; not shown), lacking either the stalk domain or both the stalk and light chain binding regions, we determined that the C-terminal cargo binding domain of KIF5 is the minimal region sufficient for mediating an interaction with HAP1, as shown by the fact that GST-HAP1 (Figure S3D) or GST-HAP1 fragments (Figure 3A–C) could readily pull down the C-terminal domain of KIF5B (residues 814–963, from here on called the HAP1-Binding Domain, or HBD; see Figure 3A). In complementary GST pull down experiments with GST-HAP1 deletion constructs (Figure 3A–C) we also determined that a region containing coiled-coil domains 1 and 2 (part of the HAP N-terminal homology domain) was sufficient for interacting with the C-terminal region of the KIF5 motor (Figure 3B&C).

We used the HAP1 binding domain of KIF5 (KIF5-HBD) as a dominant negative construct to further investigate the consequences of disrupting KIF5 dependent $GABA_A$R trafficking to synapses. Using surface biotinylation to quantify surface $GABA_A$R levels, we found that, compared to control GFP transfected neurons, neurons expressing the ^{GFP}KIF5B-HBD produced a significant decrease in the cell surface number of $GABA_A$Rs containing β3 subunits (68.5±6.0% of control, n = 8, $P < 0.005$, Figure 3D–F) whereas surface levels of either the transferrin receptor (TfR) or the NMDAR were unaffected (Figure S3E&F). The source of $GABA_A$Rs from the internal pool that supplies fast synaptic receptor insertion remains unknown. However, $GABA_A$Rs have been previously demonstrated to be rapidly re-inserted into the membrane from an intracellular pool of internalized receptors (Kittler et al., 2004). After labeling this intracellular pool of $GABA_A$Rs with biotin, the loss of biotinylated internal $GABA_A$Rs after a second biotin cleavage (see methods) provides a measure of receptor insertion rate into the membrane (Ehlers, 2000; Kittler et al., 2004). Internal biotinylated $GABA_A$Rs remaining during the time course were then compared to those at the start of the re-insertion time course (i.e. time 0 in Figure 3G), designated as 100%. We found that

expressing ^{GFP}KIF5B-HBD in neurons resulted in a significant reduction in the loss of the internal biotinylated receptor pool (i.e. more internal biotinylated receptors remained) compared to GFP controls. This gives a significant decrease in $GABA_AR$ insertion levels at 30 and 60 min upon disruption of HAP1/KIF5 dependent trafficking (Figure 3G&H: at 30 minutes 38.6±2.4% receptors remained in the internal pool for ^{GFP}KIF5B-HBD transfected neurons compared to 27.1±3.9% receptors remaining in the internal pool for GFP control transfected neurons; at 60 minutes 25.1±2.1% for ^{GFP}KIF5B-HBD compared to 14.2±2.9% for GFP control; n = 5, $P < 0.05$). In contrast $GABA_AR$ endocytosis was not affected by expressing ^{GFP}KIF5B-HBD (Figure S3G&H). Our results demonstrate that disrupting KIF5 dependent trafficking by expressing ^{GFP}KIF5B-HBD decreases receptor insertion into the surface membrane.

Functional confirmation that this decrease in trafficking resulted in a loss of synaptic receptors was observed from whole-cell patch clamp recordings (Figure 4A–E). Neurons transfected with ^{GFP}KIF5B-HBD showed a significant decrease in mIPSC amplitudes compared to GFP-transfected neurons, (Figure 4A,C&D; mean mIPSC amplitude in ^{GFP}KIF5B-HBD transfected neurons 17.8±2.4pA, n = 6, compared to 27.8±3.7pA, n = 5, for control GFP transfected neurons, significantly different, $P < 0.05$), which was also indicated by a leftward shift towards lower amplitudes in the cumulative distribution plots (Figure 4A). An even greater reduction was seen upon neuronal expression of ^{GFP}KIF5C-HBD (Figure S4A&D; ^{GFP}KIF5C-HBD: 12.7±1.2pA, n = 8, compared to GFP: 27.4±2.0pA, n = 6, $P < 0.05$; equivalent to a 53.6±4.4% reduction in mean amplitude for ^{GFP}KIF5C-HBD, compared to the 36.0±8.6% reduction seen for ^{GFP}KIF5B-HBD). In contrast ^{GFP}KIF5B-HBD or ^{GFP}KIF5C-HBD expression caused no significant alteration in mIPSC interval (Figures 4B&E and S4B&E; mIPSC average interval GFP: 0.21±0.02sec, n = 5, ^{GFP}KIF5B-HBD: 0.22±0.01sec, n = 6; GFP: 0.20±0.02sec, n = 6, ^{GFP}KIF5C-HBD: 0.24±0.01sec, n = 8). Further supporting the idea that HAP1-KIF5-dependent re-insertion of $GABA_ARs$ plays a critical role in delivery of $GABA_ARs$ to synapses, we also found that expression of KIF5-HBD decreased the size of $GABA_AR$ clusters, as demonstrated by immunofluorescence and CLSM ($GABA_AR$ cluster area in KIF5B-HBD expressing neurons was 72.9±10.3% of control GFP expressing neurons, n = 5, $P < 0.01$, see Figure 4F,G) without producing a change in the ratio of the number of synaptic to the number of non-synaptic $GABA_AR$ clusters (Figure S4F).

To further support the role of the HAP1/KIF5 complex for trafficking $GABA_ARs$ to synapses we also investigated the functional consequences of expressing in neurons the domain on HAP1 to which KIF5 binds (i.e. the HAP1-KIF5 Binding Domain; HAP1-KBD; Figure 3B). Compared to neurons expressing GFP, neurons expressing ^{GFP}HAP1-KBD showed reduced mIPSC amplitudes, (mIPSC amplitude in GFP expressing neurons 37.1±2.4 pA, n = 8 and 22.9 ±2.1 pA in ^{GFP}HAP-KBD expressing neurons, n = 7, $P < 0.01$) while similarly to expression of KIF5-HBD, mIPSC frequency remained unaffected (GFP: 5.1±0.7 Hz, n = 8; HAP1-KBD: 4.4±0.4 Hz, n = 7). In contrast to the effects observed on $GABA_AR$ mIPSC amplitude upon expression of KIF5-HBD or HAP1-KBD, targeting the function of the NMDAR motor KIF17, which does not interact with HAP1 (Figure S4L) and which blocks trafficking of NMDARs (Guillaud et al., 2003), had no effect on inhibitory synaptic function (Figure S4G–K). These results further support a critical role for the HAP1/KIF5 complex in trafficking $GABA_ARs$ to synapses.

Our results suggest that HAP1 is a specificity adaptor for the recruitment of $GABA_AR$ containing transport vesicles to a KIF5 transport pathway for their rapid delivery to synapses. To further validate the role of the HAP1-KIF5 complex we used RNA interference (RNAi) to knock down HAP1 expression (Figure 5A–C) and determined the effect on trafficking and synaptic inhibition. Similar to the effect of disrupting KIF5 function (by expressing KIF5-HBD), biotinylation experiments revealed that knocking down HAP1 (Figure 5A–C) resulted

in a substantial decrease in the number of surface $GABA_A$Rs (for HAP1 RNAi expressing neurons surface levels were 43.1±8.2% of control scrambled RNAi expressing neurons, n = 6, $P < 0.0005$, Figure 5D&E) without affecting the surface levels of TfR or the NMDAR (Figure S5A&B). Biotinylation experiments also revealed that HAP1 knockdown resulted in a significant reduction in rates of $GABA_A$R insertion into the membrane at 30 and 60 min compared to RNAi control transfected cells (Figure 5F&G). At 30 minutes the control RNAi cells had 25.3±2.6% of receptors remaining in the internal pool compared to 40.7±5.5% receptors remaining for HAP1 RNAi, while at 60 minutes the control RNAi cells had 13.0 ±2.2% receptors remaining in the internal pool compared to 25.2±5.6% in HAP1 RNAi expressing cells; n = 7–9; $P < 0.05$), but HAP1 RNAi did not alter $GABA_A$R endocytosis (Figure S5C&D). In agreement with these observations, patch clamp recordings of neurons expressing the HAP1 RNAi revealed that mIPSC amplitude, but not frequency, in neurons was dramatically reduced compared to the scrambled control RNAi (Figure 6A–E: HAP1 RNAi mIPSC amplitude, 23.7±2.1 pA, n = 8 compared to control RNAi mIPSC amplitude 41.6±2.3 pA, n = 7, $P < 0.05$; HAP1 RNAi mIPSC frequency, 4.2±0.17 Hz, n = 8 compared to control RNAi mIPSC frequency 4.2±0.25 Hz, n = 7). This correlates with the reduced size of synaptic $GABA_A$R clusters as determined by immunofluorescence and confocal imaging (70.4±8.3% of control, n = 3, $P < 0.05$, see Figure 6F&G), while no effect on the synaptic to non-synaptic ratio of $GABA_A$R cluster numbers was observed (Figure S6A).

To further study the role of HAP1 dependent $GABA_A$R trafficking we also performed live cell imaging experiments in neurons expressing GFP labeled $GABA_A$R transport vesicles. We designed a new HAP1 (or control) shRNAi vector co-expressing GFP tagged γ2 $GABA_A$R subunits ($\gamma2^{GFP}$) such that neurons expressing GFP labeled $GABA_A$Rs would also express either HAP1 RNAi or control RNAi (Figure S6B–E). By imaging over time, motile $\gamma2^{GFP}$ labeled $GABA_A$R transport vesicles in dendrites were visualized using kymographs (Figure 6I–K') that were created by projecting sequential line scans through a process of interest onto the y axis (Macaskill et al., 2009). Stationary $GABA_A$Rs are seen as straight lines and moving $GABA_A$R vesicles as diagonal lines. Using this technique, $\gamma2^{GFP}$-$GABA_A$Rs could be seen to be present in both moving and stationary clusters in dendrites. We investigated the effect of altering HAP1 expression levels on the dynamics of $\gamma2^{GFP}$-$GABA_A$R vesicle movement in neurons co-expressing HAP1 shRNAi to reduce HAP1 expression levels (Figure 6I,K). Compared to control neurons (Figure 6I,I'), far fewer $GABA_A$R vesicles could be observed to be moving, assessed over a 5 min period (Figure 6K,K'), most easily seen in the masked kymographs (bottom panels of Figure 6I'&K') which show only the tracks of moving vesicles. HAP1 knockdown also significantly affected $GABA_A$R vesicle run length with $\gamma2^{GFP}$-$GABA_A$R vesicles moving far shorter distances in the HAP1 RNAi expressing neurons than in control cells (Figure 6H; average track run length in control RNAi cells 32.9±3.1μm, and in HAP1 RNAi cells 23.6±2.9μm, $P < 0.05$, n = 45 tracks in each case).

Mutant polyQ huntingtin disrupts $GABA_A$R trafficking, synaptic receptor delivery and inhibitory transmission

HAP1 function is disrupted by the mutant (polyQ) version of huntingtin that causes Huntington's disease (Gauthier et al., 2004; Li et al., 1995). HAP1-KIF5 dependent $GABA_A$R trafficking is therefore a likely target for disruption in HD, which would lead to pathological alterations in inhibition. To further investigate this possibility we performed live cell imaging experiments in neuronal cells derived from knock-in mice, where a CAG expansion (encoding poly-glutamines) has been inserted into the endogenous mouse htt gene (Gauthier et al., 2004; Trettel et al., 2000). These cell lines reflect the closest situation to HD patients, as wild type or polyQ-htt is expressed at endogenous levels. Neuronal cells containing either two copies of wild type htt (wild-type neuronal cells, +/+), or two copies of mutant htt (homozygous mutant neuronal cells, 109Q/109Q) were transfected with GFP tagged

$GABA_ARs$ ($\alpha1\beta3\gamma2^{GFP}$) and imaged using live cell video microscopy to monitor the trafficking dynamics of $^{GFP}GABA_AR$ transport vesicles (Figure 7A–C and Movies S1 and S2). By tracking $^{GFP}GABA_AR$ transport vesicles, the influence of WT or polyQ-htt on vesicle velocity and vesicle run length was determined. These experiments revealed a significant decrease in the velocity (Figure 7A&C, 109Q/109Q cells, 0.36±0.01μm/sec compared to +/+ controls, 0.41 ±0.01μm/sec, $P < 0.05$) and run length (Figure 7B&C, 109Q/109Q cells, 5.4±0.6μm compared to +/+ cells, 7.6±0.6μm, $P < 0.05$) of $^{GFP}GABA_AR$ transport vesicles in 109Q/109Q cells compared to control +/+ cells. The effects of polyQ-htt on $^{GFP}GABA_AR$ transport vesicle dynamics were occluded by co-expression of KIF5-HBD, which reduced $GABA_AR$ vesicle trafficking to the same level in both +/+ and 109Q/109Q cells (Figure S7). Our results strongly suggest that mutant polyQ-htt causes decreased accumulation of $GABA_ARs$ at inhibitory synapses (leading to compromised inhibition) by reducing the processivity (Gauthier et al., 2004) and trafficking ability of HAP1-KIF5 dependent $GABA_AR$ transport vesicles for receptor delivery to inhibitory synapses.

To address the functional consequences of altered HAP1-KIF5-dependent $GABA_AR$ trafficking by polyQ-htt on inhibitory synaptic transmission, we transfected cortical neurons with ^{GFP}WT-htt or ^{GFP}polyQ-htt constructs and used electrophysiology to look at mIPSC properties. Compared to ^{GFP}WT-htt transfected cells, expression of ^{GFP}polyQ-htt caused a significant decrease in mIPSC amplitude (Figure 7D, F&G ^{GFP}WT-htt: 34±5.0pA, n = 6, ^{GFP}polyQ-htt: 13.7±1.4pA, n = 6, $P < 0.05$), which was also indicated by a leftward shift towards lower amplitudes in the cumulative distribution plot (Figure 7D). While polyQ-htt caused a significant reduction in mIPSC amplitude (Figure 7H, 59.7±4.1%, $P < 0.05$), it had little effect on mIPSC frequency (Figure 7E, F&H). Expressing ^{GFP}polyQ-htt also resulted in a significant decrease in the area of $GABA_AR$ clusters in neuronal dendrites compared to control ^{GFP}WT-htt transfected cells (41.5±11.5% of control, n = 5, $P < 0.01$, Figure 7I&J), but not the ratio of synaptic to non-synaptic $GABA_AR$ clusters at the cell surface (Figure S7F). These results clearly demonstrate that mutant polyQ-htt disrupts delivery of $GABA_AR$ to synapses, leading to compromised inhibitory synaptic transmission.

Discussion

We have analyzed the mechanisms that regulate the rapid transport of $GABA_ARs$ to synapses. We demonstrate that delivery of $GABA_ARs$ from internal compartments to surface and synaptic sites is dependent on a HAP1-KIF5 motor protein complex. Electrophysiological recordings in the present study provide the first evidence that KIF5-dependent trafficking of $GABA_ARs$ to synapses is a critical regulator of rapid synaptic $GABA_AR$ delivery and of the strength of the inhibitory synapses. This mechanism is likely to be a locus for regulation of trafficking of $GABA_ARs$ during inhibitory synaptic plasticity and homeostasis.

In agreement with an important role for KIF5 and HAP1 in regulating $GABA_AR$ transport, we find that $GABA_ARs$, KIF5 and HAP1 interact *in vivo* and that KIF5 is localised at inhibitory postsynaptic domains (Figure 2). Furthermore, using protein interaction mapping experiments we reveal that KIF5 heavy chains interact directly with HAP1 via a C-terminal domain in KIF5 and the central HAP1-N-terminal homology domain rich in coiled-coils (Figure 3). An earlier report demonstrated a direct interaction between a C-terminal region of HAP1 and the KLC (McGuire et al., 2005). However, we observed a much weaker direct interaction of the KLC with HAP1 compared to KIF5B and KIF5C in our pull down assay and we find the KLC binding domain of KIF5 is not necessary for the direct high affinity interaction between KIF5 heavy chains and HAP1 (Figure 2). Thus HAP1 acts as the adaptor protein directly linking $GABA_AR$ transport vesicles to KIF5 heavy chains for their trafficking along microtubules. Further work is needed to determine if KLC plays an additional regulatory role in the $GABA_AR$-HAP1-KIF5 complex. There are a large number of KIF motors (Miki et al., 2001)

and we cannot discount the possibility that other KIFs could interact with HAP1 and contribute to $GABA_AR$ trafficking. However, we show here for at least one other KIF isoform (KIF17) that a direct interaction with HAP1 was not detected, and moreover that KIF17 activity does not contribute to inhibitory synapse function, supporting the specificity of the KIF5 interaction with HAP1 and its role in $GABA_AR$ trafficking.

To test the functional significance of HAP1/KIF5 dependent $GABA_AR$ trafficking in regulating surface and synaptic $GABA_AR$ number, we examined the consequences for inhibitory synaptic currents of directly blocking KIF5 function or inhibiting the HAP1-KIF5 linkage to $GABA_ARs$. Acutely dialysing KIF5 function blocking antibody via the electrophysiological recording pipette resulted in a rapid decrease in mIPSC amplitude, demonstrating for the first time a crucial role of KIF5 motor proteins in delivering $GABA_ARs$ to synapses on rapid timescales (Figure 1). Transducing neurons with the same antibody also reduced $GABA_AR$ cluster area, as determined by immunofluorescence and CLSM. Transfection of neurons with the HAP1 binding domain of KIF5 to compete with HAP1 for binding to KIF5, or using RNAi to knockdown HAP1 and decrease the amount of HAP1-KIF5 complex present, significantly decreased surface $GABA_AR$ number, insertion of $GABA_ARs$ into the membrane from the internal pool, $GABA_AR$ cluster area and the amplitude of mIPSCs (Figure 3–Figure 6). Expressing the KIF5 binding domain of HAP1 also significantly reduced the amplitude of mIPSCs. Moreover, knockdown of HAP1 also substantially reduced the number and run length of $GABA_AR$ transport vesicles. Our observed 35–45% reduction of mIPSC size presumably reflects an action on the actively trafficked pool of receptors which is in agreement with the observed effects on receptor trafficking and receptor insertion into the membrane. In contrast, disrupting KIF5 dependent trafficking did not alter surface TfR or NMDAR levels nor the size of NMDAR responses, and blocking the function of the KIF17 motor for NMDARs did not effect GABAergic mIPSCs. Thus, the number of surface and synaptic $GABA_ARs$ can be specifically controlled by the extent of HAP1-KIF5 dependent membrane insertion of $GABA_ARs$ from the internal receptor pool to the postsynaptic membrane. In addition to being a potential locus for regulation of $GABA_AR$ trafficking during inhibitory synaptic plasticity and homeostasis, HAP1/KIF5 dependent $GABA_AR$ trafficking during the embryonic and early postnatal period, when $GABA_ARs$ can be excitatory (Ben-Ari et al., 2007), may also be important for inhibitory synapse and circuit development.

Changes in the trafficking of $GABA_ARs$ to and from the postsynaptic membrane are likely to underlie plasticity of GABAergic synapses in pathological conditions such as stroke and epilepsy, leading to alterations in inhibition and neuronal excitability (Mielke and Wang, 2005; Naylor et al., 2005). HAP1 interacts with huntingtin, the protein product mutated (by an expanded polyQ tract) in Huntington's disease. HAP1 dependent motor protein trafficking of vesicles is modified by mutant polyQ-htt and may underlie cell death in HD (Gauthier et al., 2004). Our data suggest that HAP1-KIF5 dependent $GABA_AR$ transport is disrupted by mutant polyQ-htt in HD. PolyQ-htt slowed the $GABA_AR$ vesicle transport speed, resulting in a reduced delivery and number of $GABA_ARs$ at inhibitory synapses, and a reduced inhibitory synaptic response (Figure 7). HAP1 interacts more tightly with polyQ-htt compared to wild type huntingtin (Li et al., 1995). Wild type huntingtin, via an interaction with HAP1, may be an integral component of the HAP1-KIF5 complex and traffic with $GABA_AR$ vesicles. In HD pathology, polyQ-htt may remain associated with $GABA_AR$ transport vesicles, but alter the function of the HAP1-KIF5 complex to disrupt the efficiency of $GABA_AR$ vesicle trafficking. Alternatively mutant polyQ-htt may disrupt the trafficking by sequestering HAP1 and KIF5 motors away from $GABA_AR$ transport vesicles. Further work will be needed to determine which mechanism results in mutant polyQ-htt disrupting HAP1-KIF5 dependent $GABA_AR$ trafficking.

Altered KIF5 motor protein dependent $GABA_AR$ trafficking may directly contribute to reduced synaptic inhibition and altered information processing in Huntington's disease. PolyQ-htt dependent enhancement in NMDA receptor function and trafficking are proposed to exacerbate excitotoxicity in HD (Fan et al., 2007; Zeron et al., 2002). Furthermore, increased neurotransmission and neuronal excitability are also proposed to contribute to the neuronal degeneration caused by full-length polyQ-htt early in pathology (Romero et al., 2008) and early deficits in cortical inhibition have also been reported (Gu et al., 2005). Whether polyQ-htt could also influence $GABA_AR$ trafficking, synapse development and inhibitory network function early during the development of GABAergic pathways is an interesting possibility and it is intriguing to note that in infants with early onset HD, the symptoms often include epileptic seizures (Harper, 2002). At later stages, disrupted $GABA_AR$ trafficking to synapses and compromised inhibition caused by mutant htt is likely to also inhibit a homeostatic response to potentiated excitatory synaptic activity and neuronal excitability in HD, and thus significantly contribute to pathological 'anti-homeostasis', leading to further disruption of the excitatory/inhibitory balance and increased neuronal excitotoxicity. This raises the possibility of a new therapeutic target in Huntington's disease: blocking recruitment of polyQ-htt to HAP1, so that disruption of KIF5 dependent trafficking of $GABA_ARs$ to synapses is prevented.

Methods

Details regarding antibodies, immunofluorescence staining and analysis, molecular biology and plasmid constructs are included in the Supplemental Experimental Procedures.

Electron Microscopy

Adult Sprague–Dawley rats were anesthetized with pentobarbital (60 mg/kg) and intracardially perfused with 4% paraformaldehyde (PFA) and 0.1% glutaraldehyde in PBS. After dissection, the cervical spinal cord and hippocampal tissue were kept overnight at 4°C in 4% PFA. Vibratome sections (100 μm) were cryoprotected for 3h in 20% glycerol and 20% sucrose at room temperature. They were then permeabilized by freeze-thawing, extensively rinsed in PBS and immersed for 20 min in 50 mM ammonium chloride and for 30 min in PBS with 0.1% gelatin (PBSg). For immunogold detection of KIF5, vibratome sections were incubated for 12 hours (4°C) in the anti-KIF5 antibody and antibody binding sites detected using secondary nanogold-coupled antibody (1% in PBSg, Nanoprobe, Stony Brook, New York). Gold particles were intensified with HQ silver kit (Nanoprobe) and subsequently gold-toned (Gardiol et al., 1999). Immunoperoxidase methods (Colin et al., 1998) were used for the detection of GAD and KIF5C. For double detection of KIF5 and GAD (Figure 2E,F) the KIF5 detection procedure was performed first. After gold toning, the sections were subsequently kept overnight (4°C) in anti-GAD before immunoperoxidase detection. After dehydration and osmification, the sections were flat-embedded. Observations of ultrathin sections (pale yellow) were contrasted with uranyl acetate and Reynolds lead citrate (Poole, UK). Images were collected with a JEOL 100CXII electron microscope (Paris, France).

Immunoprecipitation assays from rat brain homogenates

Adult rat brains were homogenised on ice in 10ml of buffer (50mM HEPES pH 7.5, 0.5% triton-X-100, 150mM NaCl, 1mM EDTA, 1mM PMSF in the presence of antipain, pepstatin and leupeptin) then left to rotate at 4°C for 2 hours. Membranes were pelleted by ultracentrifugation at ~66000g for 40 minutes at 4°C. Protein content of the supernatant was assayed by BioRad protein assay. 2 to 5mg of protein was transferred to a 1.5ml microcentrifuge tube and made up to 500μl with homogenisation buffer. For co-immunoprecipitations 1–2μCg of a primary antibody was added in parallel to a suitable non-immune IgG control antibody (Santa Cruz Biotechnology) of the same species. Samples were incubated overnight at 4°C with rotation. Complexes were precipitated with 15μl of 50% protein A (for rabbit antibodies)

or protein G (for goat antibodies) sepharose bead slurry (Generon) for one hour at 4°C. Beads were then washed 3 times by centrifugation and resuspension in 1ml of homogenisation buffer. Samples were suspended in 3× protein sample buffer and analysed by SDS-PAGE and western blotting.

Pull down assays

Affinity purifications, using GST-fusion proteins purified from *E. Coli*, were performed as described in a number of previous studies (see refs (Kittler et al., 2005; Kittler et al., 2000a)). For pull downs from rat brain, 50μg of GST fusion protein immobilised on agarose beads was incubated in rat brain homogenate for 2 hours at 4°C, followed by 5 washes in homogenisation buffer. Complexes were washed five times with pull down buffer and then analysed by SDS-PAGE and Western blotting. For pull downs from transfected COS cells, transfected cells were harvested 24 hours post transfection. 10cm dishes of COS cells were solubilised in 0.5ml of pull down buffer (50mM HEPES pH 7.5, 0.5% triton, 150mM NaCl, 1mM EDTA, 1mM PMSF in the presence of antipain, pepstatin and leupeptin) for 45 minutes at 4°C. Detergent solubilised extracts were collected following centrifugation for 10 minutes at 17,900g, 4°C, placed in a fresh 1.5ml microcentrifuge tube and incubated with 20μg of GST fusion protein for two hours. Complexes were washed five times with pull down buffer and then analysed by SDS-PAGE and Western blotting with mouse anti-GFP (Roche). For pull downs with radiolabelled protein, KIF5A, KIF5B, KIF5C and KLC1 were in vitro translated (IVT) from their appropriate pRK5 vectors using TNT® SP6 Quick coupled Transcription/Translation system (Promega) and labelled with [^{35}S]-Methionine (Perkin Elmer) following the manufacturer's instructions, with a 50μl final volume. 10 to 15μl of IVT S^{35} labelled protein was incubated for 2 hours with 10μg of GST fusion protein immobilised on glutathione agarose beads in a final volume of 500μl, diluted in pull down buffer. Complexes were washed three times in pull down buffer and resolved by SDS-PAGE. Gels were dried and radioactivity detected using a storage phosphor screen.

Cell culture, transfection and transduction

COS and HEK cells were maintained as described previously and transfected using electroporation (Kittler et al., 2000a; Kittler et al., 2000b). The neuronal cells (109Q/109Q and +/+) derived from knock in mice (Gauthier et al., 2004; Trettel et al., 2000) were cultured in DMEM supplemented with 10% FBS, PenStrep, 40μg/ml G418, 1% glutamine and sodium pyruvate. Cortical, hippocampal and striatal cultures were isolated from E18 or P0 Sprague-Dawley rats as described in a number of previous publications (Banker and Goslin, 1998; Chen et al., 2006; Kittler et al., 2004; Macaskill et al., 2009). Cultures for biotinylation experiments were transfected using Amaxa nucleofector technology using programme O-003 and plated onto poly-L-lysine prepared 10cm dishes. +/+ and 109Q/109Q cultures for live video microscopy were transfected using Amaxa nucleofector technology using programme T27 and plated onto coverslips for imaging. Cultures for surface labelling and analysis of $GABA_AR$ clusters were transfected by a calcium phosphate method as previously described (Kittler et al., 2006) at 7–10 DIV and allowed to express for at least three days before fixation. Monoclonal antibodies (affinity purified SUK4, or 9E10 antibody as a control) were transduced across the plasma membrane of DIV 10–14 neurons using Chariot reagent (Active Motif) following the manufacturer's instructions with minor modifications (Coulpier et al., 2002; Kittler et al., 2006; Ma et al., 2006). In brief, per well of a 24 well plate, 2μl of Chariot reagent was diluted in 50μl of water before pre-complexing with 20μg of antibody in 50μl of PBS for 30 minutes. The 100μl of complexed antibody/chariot was then overlaid onto the cultured neurons with 100μl of fresh complete neuronal culture medium and left to incubate at 37°C for 1 hour. Another 400μl of fresh medium was then overlaid on the neurons and incubation was continued for 12 hours before cells were fixed and stained (see Supplemental Experimental Procedures).

Video Microscopy

All live imaging of transfected $GABA_A$Rs was performed in imaging media (10mM HEPES pH7.4, 125mM NaCl, 5mM KCl, 2mM $CaCl_2$, 1mM $MgCl_2$, 10mM D-glucose, 285–300 mOsm) at 35–37°C under constant perfusion using an Ixon EM-CCD camera (Andor) on an upright Olympus BX51WI microscope. 109Q/109Q and +/+ neuronal cell lines were transfected with either $\alpha\beta\gamma^{GFP}$ or $\alpha\beta\gamma^{dsRed}$ with ^{GFP}KIF5B-HBD or pEGFP and movies were captured at 0.5 or 2 Hz. Movies of calcium phosphate transfected cultured cortical neurons were captured at 1 Hz. Illumination was provided by a high intensity arc lamp with GFP visualised with an excitation filter of 470nm (bandwidth 40nm) and an emission filter of 525nm (bandwidth 40nm) and DsRed visualized with an excitation filter of 535nm (bandwidth 40nm) and an emission filter 620nm (bandwidth 40nm). Vesicle velocities were calculated from captured movies by analyses with either the 'Track Points' macro of Metamorph (Universal Imaging) or ImageJ software using plugins available from the ImageJ website (http://rsb.info.nih.gov/ij/plugins/) as follows. To readily identify vesicles over a noisy background in neurons images were filtered using the spot enhancer filter from the SpotTracker plugin (D. Sage). Where coverslip drift was visible, images were corrected with the Stackreg plugin (P. Thevenas). Individual moving vesicles were tracked manually using Mtrack J plugin (E. Meijering). Kymographs were made using the multiple kymograph function. For mitochondrial velocity measurements, striatal cells were transfected with mtDsRed2 (Clontech). This construct contains DsRed fluorescent protein targeted to mitochondria via the targeting peptide of cytochrome oxidase. Cells were imaged under constant perfusion of imaging media at 36°C using a Zeiss Pascal upright confocal microscope and LSM software with an Achroplan 63× water-immersion lens with 0.95 numerical aperture. Images were acquired at 1 Hz. Excitation was via a HeNe laser at lambda = 543 nm. Mitochondrial velocity was measured as for vesicles above.

Surface biotinylation assay

Nucleofected cultured cortical cultures were kept at 4°C and rinsed with PBS (all washing steps were performed in PBS supplemented with 1 mM $CaCl_2$ and 0.5 mM $MgCl_2$) before incubation with 0.5 mg/ml EZ-Link Sulfo-NHS-SS-Biotin (Pierce) for 12 minutes. The surface biotinylation reaction was quenched using three washes of 1 mg/ml BSA in Mg^{2+}/Ca^{2+} supplemented PBS. Cells were washed and solubilised in 360µl of RIPA buffer (50 mM Tris pH 7.5, 1 mM EDTA, 2 mM EGTA, 150 mM NaCl, 1% NP40, 0.5% DOC, 0.1% SDS, 1 mM PMSF with antipain, pepstatin and leupeptin) for 1 hour at 4°C. Cell membranes were pelleted at 14,000 rpm for 10 minutes at 4°C. 60µl (20%) was kept to analyse as an input. The remainder was incubated with 50µl of UltraLink NeutrAvidin bead slurry (Pierce) for 2 hours at 4°C. Beads were washed twice with high salt (0.5 M NaCl) RIPA buffer and once with normal (0.15 M NaCl) RIPA buffer. Complexes were separated by SDS-PAGE and analysed by Western blotting. $GABA_A$Rs were detected with rabbit anti-$GABA_A$R-β3 subunit as primary antibody and [125I]-labelled donkey anti-rabbit (Perkin Elmer) as secondary antibody. Radioactivity of Western blots was detected using a storage phosphor screen.

For biotin endocytosis assays, nucleofected cortical cultures were surface biotinylated as above and following quenching, media was returned to the dishes and neurons were incubated at 37° C for 30 minutes to allow internalisation. Cleavage of remaining surface biotin was carried out at 4°C by two 15 minute incubations in cleavage solution (50mM glutathione, 10mM EDTA, 75mM NaCl, 1% BSA, pH 7.8). Cultures were solubilised and complexes precipitated as for surface biotinylations. Re-insertion biotinylation assays of cortical cultures were performed as described previously (Kittler et al., 2004). Briefly, cortical neurons were labeled with biotin and receptors were allowed to internalize for 30 min [the period for maximal receptor internalization (Kittler et al., 2004)], before cleavage with glutathione. Neurons were then incubated at 37°C for further time periods with glutathione in the external culture medium to

cleave any internalized biotinylated receptors recycling to the cell surface. The loss of biotinylated internalized $GABA_A$Rs after the second biotin cleavage provides a measure of receptor recycling (Ehlers, 2000). Internal β3-subunit levels remaining were then compared to those at the start of the second incubation period with glutathione, designated as 100%.

Whole-cell recordings

Whole-cell recordings of mIPSCs from cultured neurons were performed using standard voltage clamp techniques (Chen et al., 2006; Kittler et al., 2004). Electrodes were filled with the following internal solution: 100 mM CsCl, 30 mM N-methyl-D-glucamine, 10 mM HEPES, 1 mM $MgCl_2$, 1 mM EGTA, 5 mM QX314, 12 mM phosphocreatine, 5 mM MgATP, 1.5 mM Na_2GTP, 0.1 mM leupeptin, pH = 7.2–7.3, 265– 270 mOsm/liter. The neurons were recorded in tetrodotoxin (0.5 μM) and held at −70mV. Recordings of whole-cell ion channel currents used standard voltage-clamp techniques as described previously (Yuen et al., 2008; Yuen et al., 2005). The internal solution contains the following: 180 mM N-methyl-D-glucamine, 40 mM HEPES, 4 mM $MgCl_2$, 0.5 mM BAPTA, 12 mM phosphocreatine, 3 mM Na_2ATP, 0.5 mM Na_2GTP, and 0.1 mM leupeptin, pH 7.2–7.3 (265–270 mOsm/l). The external solution consisted of the following: 127 mM NaCl, 20 mM CsCl, 10 mM HEPES, 1 mM $CaCl_2$, 5 mM $BaCl_2$, 12 mM glucose, 0.001 mM TTX, and 0.02 mM glycine, pH 7.3–7.4 (300–305 mOsm/l). GABA (100 μM) or NMDA (100 μM) was applied for 2 s every 30 s via a gravity-fed “sewer pipe” system using capillaries (150 μm inner diameter) positioned a few hundred micrometers from the neuron under study. The membrane holding potential was −40mV and −70mV for GABA and NMDA currents, respectively. Data were analysed with Axograph (Axon Instruments, Union City, CA), Kaleidagraph (Albeck Software, Reading, PA) and Mini Analysis program (Synaptosoft, Leonia, NJ).

Supplementary Material

Refer to Web version on PubMed Central for supplementary material.

Acknowledgments

JTK is supported by the U.K. Medical Research Council. We also acknowledge support from the European Commission Coordination Action ENINET (contract number LSHM-CT-2005-19063). We are very grateful to Marcie MacDonald and Elisa Fossale for generously providing the striatal wild type and 109Q knock in cells and Anne Stephenson for providing the KIF5C-MD and -NMD constructs. We thank James Muir and David Attwell for comments on the manuscript.

References

Arancibia-Carcamo IL, Kittler JT. Regulation of GABA(A) receptor membrane trafficking and synaptic localization. Pharmacol Ther 2009;123:17–31. [PubMed: 19374920]

Banker, G.; Goslin, K. Culturing nerve cells. 2nd edn. Massachusetts: The MIT Press; 1998.

Ben-Ari Y, Gaiarsa JL, Tyzio R, Khazipov R. GABA: a pioneer transmitter that excites immature neurons and generates primitive oscillations. Physiol Rev 2007;87:1215–1284. [PubMed: 17928584]

Bi GQ, Morris RL, Liao G, Alderton JM, Scholey JM, Steinhardt RA. Kinesin- and myosin-driven steps of vesicle recruitment for Ca2+-regulated exocytosis. The Journal of cell biology 1997;138:999–1008. [PubMed: 9281579]

Chen G, Kittler JT, Moss SJ, Yan Z. Dopamine D3 receptors regulate GABAA receptor function through a phospho-dependent endocytosis mechanism in nucleus accumbens. J Neurosci 2006;26:2513–2521. [PubMed: 16510729]

Colin I, Rostaing P, Augustin A, Triller A. Localization of components of glycinergic synapses during rat spinal cord development. J Comp Neurol 1998;398:359–372. [PubMed: 9714149]

Coulpier M, Anders J, Ibanez CF. Coordinated activation of autophosphorylation sites in the RET receptor tyrosine kinase: importance of tyrosine 1062 for GDNF mediated neuronal differentiation and survival. J Biol Chem 2002;277:1991–1999. [PubMed: 11713247]

Dumoulin A, Rostaing P, Bedet C, Levi S, Isambert MF, Henry JP, Triller A, Gasnier B. Presence of the vesicular inhibitory amino acid transporter in GABAergic and glycinergic synaptic terminal boutons. J Cell Sci 1999;112(Pt 6):811–823. [PubMed: 10036231]

Ehlers MD. Reinsertion or degradation of AMPA receptors determined by activity-dependent endocytic sorting. Neuron 2000;28:511–525. [PubMed: 11144360]

Engelender S, Sharp AH, Colomer V, Tokito MK, Lanahan A, Worley P, Holzbaur EL, Ross CA. Huntingtin-associated protein 1 (HAP1) interacts with the p150Glued subunit of dynactin. Hum Mol Genet 1997;6:2205–2212. [PubMed: 9361024]

Fan MM, Fernandes HB, Zhang LY, Hayden MR, Raymond LA. Altered NMDA receptor trafficking in a yeast artificial chromosome transgenic mouse model of Huntington's disease. J Neurosci 2007;27:3768–3779. [PubMed: 17409241]

Fan MM, Raymond LA. N-methyl-D-aspartate (NMDA) receptor function and excitotoxicity in Huntington's disease. Progress in neurobiology 2007;81:272–293. [PubMed: 17188796]

Gardiol A, Racca C, Triller A. Dendritic and postsynaptic protein synthetic machinery. J Neurosci 1999;19:168–179. [PubMed: 9870948]

Gauthier LR, Charrin BC, Borrell-Pages M, Dompierre JP, Rangone H, Cordelieres FP, De Mey J, MacDonald ME, Lessmann V, Humbert S, Saudou F. Huntingtin controls neurotrophic support and survival of neurons by enhancing BDNF vesicular transport along microtubules. Cell 2004;118:127–138. [PubMed: 15242649]

Gu X, Li C, Wei W, Lo V, Gong S, Li SH, Iwasato T, Itohara S, Li XJ, Mody I, et al. Pathological cell-cell interactions elicited by a neuropathogenic form of mutant Huntingtin contribute to cortical pathogenesis in HD mice. Neuron 2005;46:433–444. [PubMed: 15882643]

Guillaud L, Setou M, Hirokawa N. KIF17 dynamics and regulation of NR2B trafficking in hippocampal neurons. J Neurosci 2003;23:131–140. [PubMed: 12514209]

Gunawardena S, Her LS, Brusch RG, Laymon RA, Niesman IR, Gordesky-Gold B, Sintasath L, Bonini NM, Goldstein LS. Disruption of axonal transport by loss of huntingtin or expression of pathogenic polyQ proteins in Drosophila. Neuron 2003;40:25–40. [PubMed: 14527431]

Harper, PS. Huntington's Disease. Vol. Vol 45. London: Oxford University Press; 2002.

Hirokawa N, Takemura R. Molecular motors and mechanisms of directional transport in neurons. Nature reviews 2005;6:201–214.

Ingold AL, Cohn SA, Scholey JM. Inhibition of kinesin-driven microtubule motility by monoclonal antibodies to kinesin heavy chains. The Journal of cell biology 1988;107:2657–2667. [PubMed: 2974459]

Jacob TC, Moss SJ, Jurd R. GABA(A) receptor trafficking and its role in the dynamic modulation of neuronal inhibition. Nature reviews 2008;9:331–343.

Jaulin F, Xue X, Rodriguez-Boulan E, Kreitzer G. Polarization-dependent selective transport to the apical membrane by KIF5B in MDCK cells. Dev Cell 2007;13:511–522. [PubMed: 17925227]

Kittler JT, Chen G, Honing S, Bogdanov Y, McAinsh K, Arancibia-Carcamo IL, Jovanovic JN, Pangalos MN, Haucke V, Yan Z, Moss SJ. Phospho-dependent binding of the clathrin AP2 adaptor complex to GABAA receptors regulates the efficacy of inhibitory synaptic transmission. Proc Natl Acad Sci U S A 2005;102:14871–14876. [PubMed: 16192353]

Kittler JT, Delmas P, Jovanovic JN, Brown DA, Smart TG, Moss SJ. Constitutive endocytosis of GABAA receptors by an association with the adaptin AP2 complex modulates inhibitory synaptic currents in hippocampal neurons. J Neurosci 2000a;20:7972–7977. [PubMed: 11050117]

Kittler, JT.; Hanley, JG.; Issac, JTR. Transfecting and transducing neurons with synthetic nucleic acids and biologically active macromolecules. In: Kittler, JT.; Moss, SJ., editors. The Dynamic Synapse: Molecular Methods in Ionotropic Receptor Biology. 2006. (CRC Press)

Kittler JT, Thomas P, Tretter V, Bogdanov YD, Haucke V, Smart TG, Moss SJ. Huntingtin-associated protein 1 regulates inhibitory synaptic transmission by modulating gamma-aminobutyric acid type A receptor membrane trafficking. Proc Natl Acad Sci U S A 2004;101:12736–12741. [PubMed: 15310851]

Kittler JT, Wang J, Connolly CN, Vicini S, Smart TG, Moss SJ. Analysis of GABAA receptor assembly in mammalian cell lines and hippocampal neurons using gamma 2 subunit green fluorescent protein chimeras. Mol Cell Neurosci 2000b;16:440–452. [PubMed: 11085880]

Lane JD, Allan VJ. Microtubule-based endoplasmic reticulum motility in Xenopus laevis: activation of membrane-associated kinesin during development. Mol Biol Cell 1999;10:1909–1922. [PubMed: 10359605]

Li SH, Gutekunst CA, Hersch SM, Li XJ. Interaction of huntingtin-associated protein with dynactin P150Glued. J Neurosci 1998;18:1261–1269. [PubMed: 9454836]

Li XJ, Li SH. HAP1 and intracellular trafficking. Trends Pharmacol Sci 2005;26:1–3. [PubMed: 15629196]

Li XJ, Li SH, Sharp AH, Nucifora FC Jr, Schilling G, Lanahan A, Worley P, Snyder SH, Ross CA. A huntingtin-associated protein enriched in brain with implications for pathology. Nature 1995;378:398–402. [PubMed: 7477378]

Ma Y, Li J, Chiu I, Wang Y, Sloane JA, Lu J, Kosaras B, Sidman RL, Volpe JJ, Vartanian T. Toll-like receptor 8 functions as a negative regulator of neurite outgrowth and inducer of neuronal apoptosis. The Journal of cell biology 2006;175:209–215. [PubMed: 17060494]

Macaskill AF, Rinholm JE, Twelvetrees AE, Arancibia-Carcamo IL, Muir J, Fransson A, Aspenstrom P, Attwell D, Kittler JT. Miro1 is a calcium sensor for glutamate receptor-dependent localization of mitochondria at synapses. Neuron 2009;61:541–555. [PubMed: 19249275]

McGuire JR, Rong J, Li SH, Li XJ. Interaction of huntingtin-associated protein-1 with kinesin light chain: Implications in intracellular trafficking in neurons. J Biol Chem. 2005

Mielke JG, Wang YT. Insulin exerts neuroprotection by counteracting the decrease in cell-surface GABA receptors following oxygen-glucose deprivation in cultured cortical neurons. J Neurochem 2005;92:103–113. [PubMed: 15606900]

Miki H, Setou M, Kaneshiro K, Hirokawa N. All kinesin superfamily protein, KIF, genes in mouse and human. Proc Natl Acad Sci U S A 2001;98:7004–7011. [PubMed: 11416179]

Morris MC, Depollier J, Mery J, Heitz F, Divita G. A peptide carrier for the delivery of biologically active proteins into mammalian cells. Nature biotechnology 2001;19:1173–1176.

Naylor DE, Liu H, Wasterlain CG. Trafficking of GABA(A) receptors, loss of inhibition, and a mechanism for pharmacoresistance in status epilepticus. J Neurosci 2005;25:7724–7733. [PubMed: 16120773]

Olkkonen VM, Ikonen E. When intracellular logistics fails--genetic defects in membrane trafficking. J Cell Sci 2006;119:5031–5045. [PubMed: 17158910]

Romero E, Cha GH, Verstreken P, Ly CV, Hughes RE, Bellen HJ, Botas J. Suppression of neurodegeneration and increased neurotransmission caused by expanded full-length huntingtin accumulating in the cytoplasm. Neuron 2008;57:27–40. [PubMed: 18184562]

Setou M, Nakagawa T, Seog DH, Hirokawa N. Kinesin superfamily motor protein KIF17 and mLin-10 in NMDA receptor-containing vesicle transport. Science 2000;288:1796–1802. [PubMed: 10846156]

Smith R, Brundin P, Li JY. Synaptic dysfunction in Huntington's disease: a new perspective. Cell Mol Life Sci 2005;62:1901–1912. [PubMed: 15968465]

Szebenyi G, Morfini GA, Babcock A, Gould M, Selkoe K, Stenoien DL, Young M, Faber PW, MacDonald ME, McPhaul MJ, Brady ST. Neuropathogenic forms of huntingtin and androgen receptor inhibit fast axonal transport. Neuron 2003;40:41–52. [PubMed: 14527432]

Trettel F, Rigamonti D, Hilditch-Maguire P, Wheeler VC, Sharp AH, Persichetti F, Cattaneo E, MacDonald ME. Dominant phenotypes produced by the HD mutation in STHdh(Q111) striatal cells. Hum Mol Genet 2000;9:2799–2809. [PubMed: 11092756]

Yuen EY, Jiang Q, Chen P, Feng J, Yan Z. Activation of 5-HT2A/C receptors counteracts 5-HT1A regulation of n-methyl-D-aspartate receptor channels in pyramidal neurons of prefrontal cortex. J Biol Chem 2008;283:17194–17204. [PubMed: 18442977]

Yuen EY, Jiang Q, Chen P, Gu Z, Feng J, Yan Z. Serotonin 5-HT1A receptors regulate NMDA receptor channels through a microtubule-dependent mechanism. J Neurosci 2005;25:5488–5501. [PubMed: 15944377]

Zeron MM, Hansson O, Chen N, Wellington CL, Leavitt BR, Brundin P, Hayden MR, Raymond LA. Increased sensitivity to N-methyl-D-aspartate receptor-mediated excitotoxicity in a mouse model of Huntington's disease. Neuron 2002;33:849–860. [PubMed: 11906693]

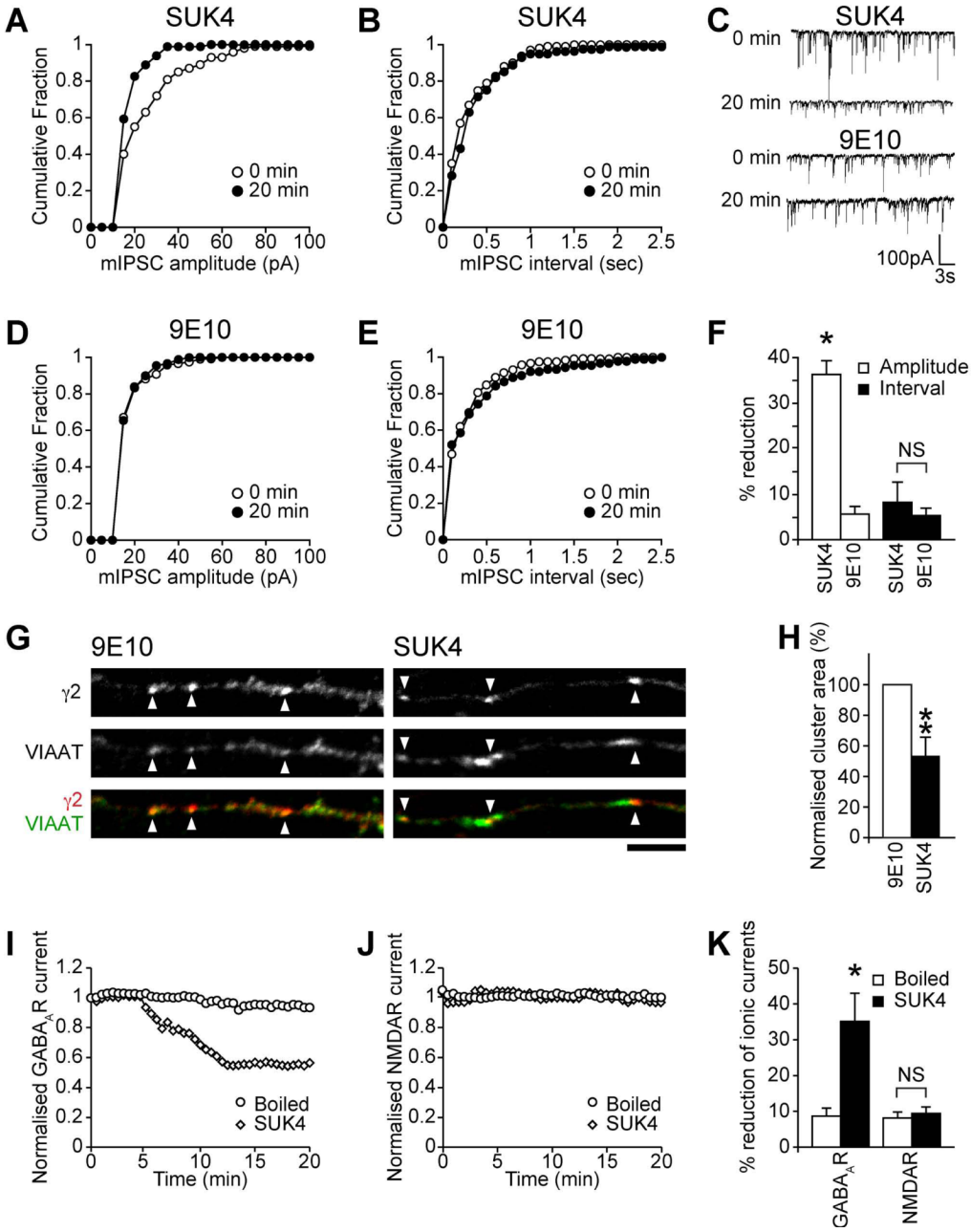

Figure 1. KIF5 delivers GABA$_A$Rs to synapses

(A–F) mIPSCs in neurons dialyzed with either SUK4 or control 9E10 antibodies. Cumulative distribution plots show mIPSC amplitudes shifted leftward in SUK4-dialyzed (A) but not control 9E10 dialyzed (D) neurons at t = 20 compared to t = 0 min. There is no change in mIPSC interval for either SUK4 or 9E10 (B, E). Representative traces reveal time-dependent reduction in mIPSC sizes upon dialysis of SUK4, but not control 9E10 antibody (C). Summary bar graphs (F) show the percentage (mean ± s.e.m.) reduction of mIPSC amplitude and interval produced by SUK4 or 9E10 after 20 minutes of antibody dialysis (SUK4, n = 7; 9E10, n = 5; *, $P < 0.05$).

(G, H) Immunofluorescence and CLSM reveals that SUK4 treatment of neurons reduces synaptic $GABA_AR$ cluster area (arrowheads) compared to 9E10 control (scale bar = 5μm). Error bars, s.e.m.; n = 3 experiments, 15 neurons; **, $P < 0.01$, (Students *t*-test). (I–K) Evoked whole cell recordings of $GABA_AR$ currents (I) and NMDAR currents (J) were recorded from neurons dialyzed with either the SUK4 or boiled (inactive) antibody control. SUK4 antibody caused a gradual reduction on $GABA_AR$ currents, but the boiled antibody control had no affect. Dialysis of either antibody failed to affect NMDAR currents. (K) Summary bar graph showing the percentage reduction in ionic currents. Error bars, s.e.m.; n = 6–7; *. $P < 0.05$.

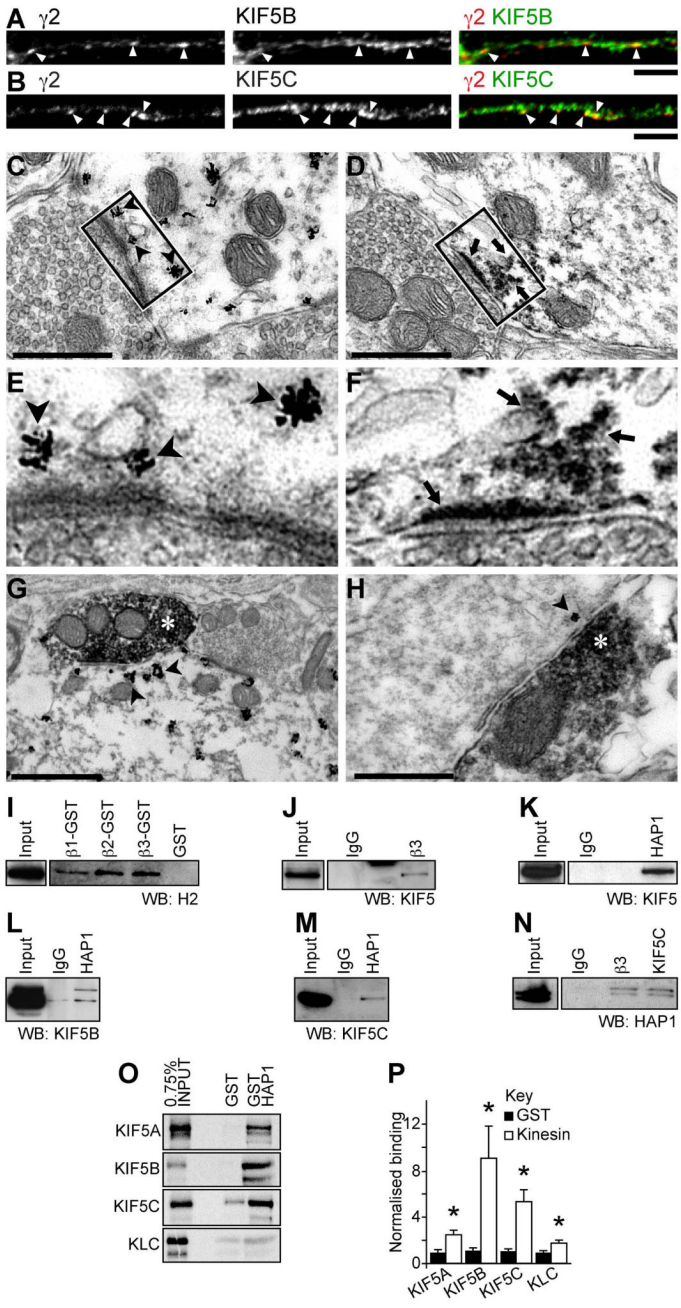

Figure 2. Endogenous HAP1/KIF5/GABA$_A$R complexes

(A–H) KIF5 colocalises with GABA$_A$Rs and is found at inhibitory post-synapses. (A, B) Neurons co-stained with antibodies to the GABA$_A$R γ2 subunit and either anti-KIF5B (A) or anti-KIF5C (B) (green; scale bar = 5μm). Both KIF5B and KIF5C are found to colocalize (yellow) with a subset of γ2 containing GABA$_A$R clusters in dendrites (arrowheads). (C–H) Ultrastructural localization of KIF5 heavy chains (scale bars, C, D & H = 0.5μm; G = 1μm). Discontinuous deposits of gold-toned silver-intensified nanogold particles immunolabelling KIF5 (C, E, G & H arrowheads) or electron dense HRP reaction product (D and F, arrows) are frequently seen close to the postsynaptic membrane opposed to presynaptic boutons containing pleiomorphic populations of vesicles indicative of inhibitory synapses (C,

D, E & F) or GAD HRP immunolabelled boutons (G & H, white star, from spinal cord and hippocampal tissue respectively). (D) KIF5C localised at the inhibitory postsynaptic membrane. (E) Boxed region in C. (F) Boxed region in D. (E and F) KIF5 is frequently seen associated with vesicles close to the postsynaptic membrane.

(I–N) Co-precipitation and pull down assays of $GABA_A$Rs, KIF5 and HAP1 from rat brain reveals they form complexes *in vivo* (WB = Western Blot; Input = 5–15% of the brain lysate present in the assay; each blot represents at least 3 repetitions). Western blots of pull downs with GST fusion proteins of the intracellular loops of $GABA_A$R subunits β1, 2 and 3 show they were able to bring down kinesin heavy chains (I) as was immunoprecicitation with antibodies against the β3 subunits of $GABA_A$Rs (J). HAP1 antibodies also immunoprecipitate KIF5 when western blots are probed with a pan KIF5 antibody (K) or with specific antibodies against both KIF5B (L) and KIF5C (M). In reverse immunoprecipitation experiments with anti-$GABA_A$R β3 antibodies and anti-KIF5C, HAP1a and HAP1b are present in immune pellets (N).

(O, P) The kinesin motor subunits KIF5A–C and kinesin light chain (KLC) were translated in vitro and labelled with [^{35}S]-methionine. The resulting protein was subjected to pull down assay with GST-HAP1, and GST alone as control, separated by SDS-PAGE (O) and radioactivity detected using a phosphor storage screen. (P) Summary bar graph of relative binding of KIF5 subunits to HAP1. Error bars, s.e.m.; n = 5; *, $P < 0.05$, Students *t*-test.

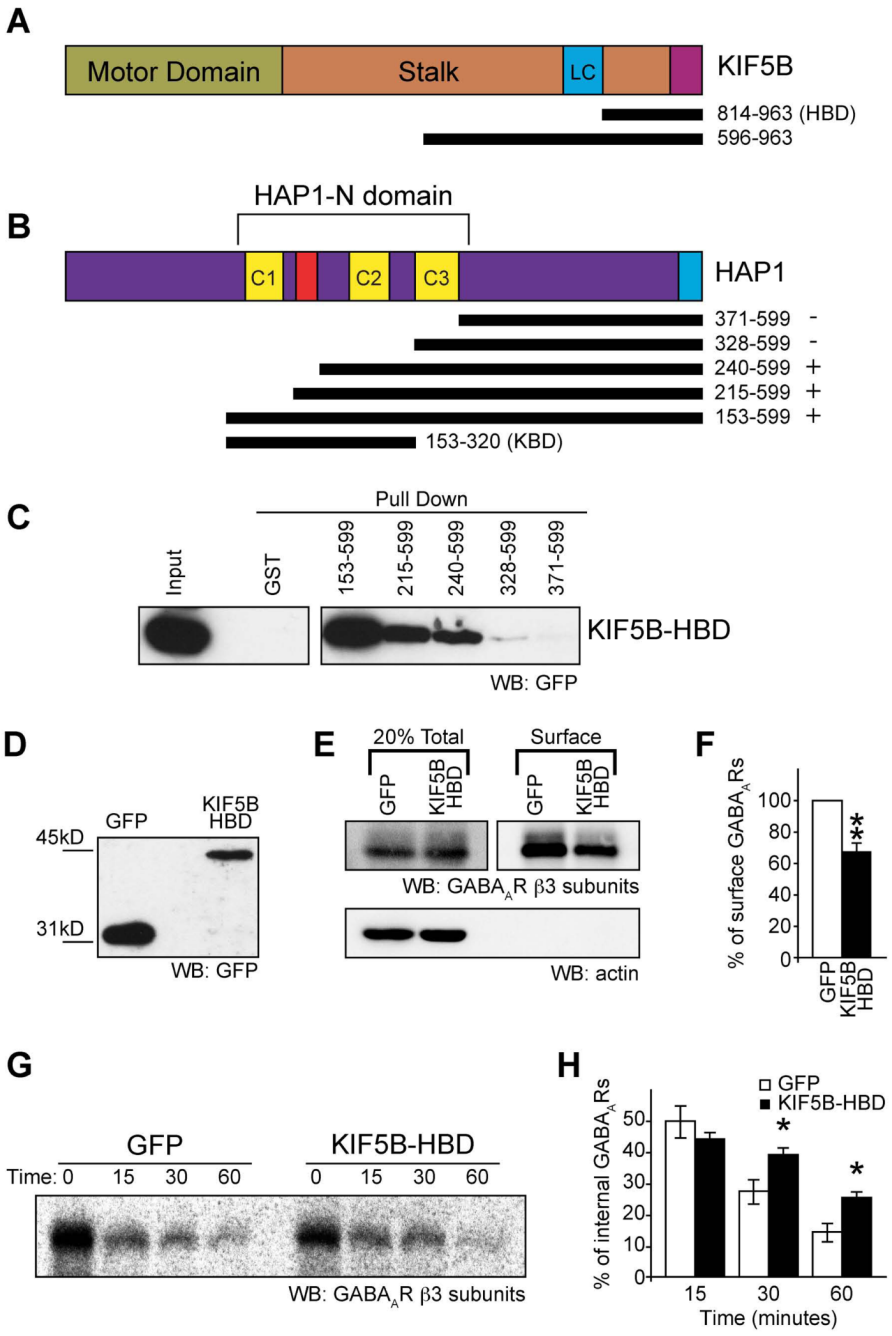

Figure 3. A HAP1-KIF5 complex mediates re-insertion of GABA$_A$Rs from the intracellular pool into the surface membrane

(A–C) Identification of the binding sites on HAP1 and KIF5. (A,B) Schematic diagrams of KIF5 and HAP1 constructs relative to the full-length proteins. (C) ^{GFP}KIF5B residues 814–963 (designated KIF5B-HAP1 Binding Domain: KIF5B-HBD) is sufficient for binding to a central region of HAP1 (residues 153–328) in a pull down assay.

(D) GFP and ^{GFP}KIF5B-HBD expression in lysates from transfected neurons used for biotinylation assays (E–H) detected by western blotting (WB) with GFP antibodies.

(E, F) Expression of KIF5B-HBD reduces surface expression of GABA$_A$Rs in neurons as revealed by surface biotinylation and western blotting with anti-GABA$_A$R-β3 subunit

antibodies. Surface receptors were labelled with biotin and surface expression normalised to the total number of receptors in the system. Actin blot (lower panel, E) shows actin present in total lysates (the saved 20% fraction) of cells, but exclusion from the surface only biotinylated fraction. (F) Summary bar graph shows surface expression normalised to GFP control (n = 8 experiments; Error bars, s.e.m.; ** $P < 0.005$, Students *t*-test).

(G,H) Expression of KIF5-HBD reduces re-insertion of internalised $GABA_A$Rs. (G) A representative western blot of the re-insertion time course, bands represent the protected internal pool of $GABA_A$Rs following 0, 15, 30 and 60 minutes of re-insertion. The loss of biotinylated $GABA_A$Rs provides a measure of receptor re-insertion. (H) Expression of ^{GFP}KIF5B-HBD causes a reduced rate of reinsertion shown by increased levels of internal receptors at 30 and 60 minute time points (n = 5; Error bars, s.e.m.; *, $P < 0.05$, Students *t*-test)

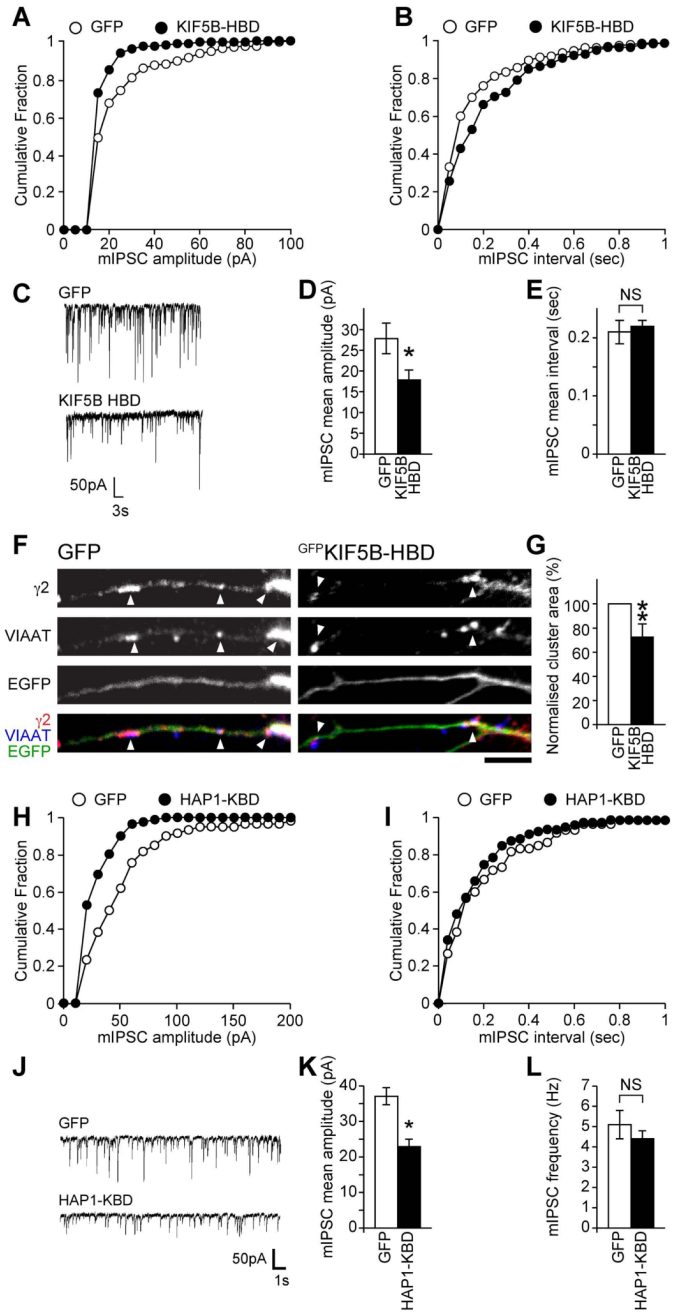

Figure 4. A HAP1-KIF5 complex can modulate inhibitory synaptic transmission

(A–E) Whole-cell recordings of mIPSCs from neurons transfected with ^{GFP}KIF5B-HBD or GFP control. (C) Representative traces demonstrating reduction in mIPSC amplitudes in cells transfected with ^{GFP}KIF5B-HBD compared to GFP-transfected cells. Cumulative distribution plots show the mIPSC amplitude shifts to smaller amplitudes in neurons transfected with ^{GFP}KIF5B-HBD (A), whilst there is no change in mIPSC interval (B). Summary bar graphs (D, E) show the average (mean ± s.e.m.) mIPSC amplitude and interval of transfected neurons (GFP, n = 5; KIF5B-HBD, n = 6; *, $P < 0.05$).

(F, G) $GABA_AR$ cluster analysis reveals that neurons expressing KIF5B-HBD^{GFP} show reduction in synaptic γ2 clusters (arrowheads) compared to GFP control expressing cells (scale

bar = 5 μm). Error bars, s.e.m.; n = 5 experiments, 26–27 neurons; **: $P < 0.01$, (Students *t*-test).

(H–L) Whole-cell recordings of mIPSCs from neurons transfected with ^{GFP}HAP1-KBD or GFP control. (J) Representative traces demonstrating reduction in mIPSC amplitude in cells transfected with ^{GFP}HAP1-KBD compared to GFP-transfected cells. Cumulative distribution plots show the mIPSC amplitude shifts to smaller amplitudes in neurons transfected with ^{GFP}HAP1-KBD (H), whilst there is no change in mIPSC interval (I). Summary bar graphs (K, L) show the average (mean ± s.e.m.) mIPSC amplitude and frequency of transfected neurons (GFP, n = 8; HAP1-KBD, n = 7; *, $P < 0.05$).

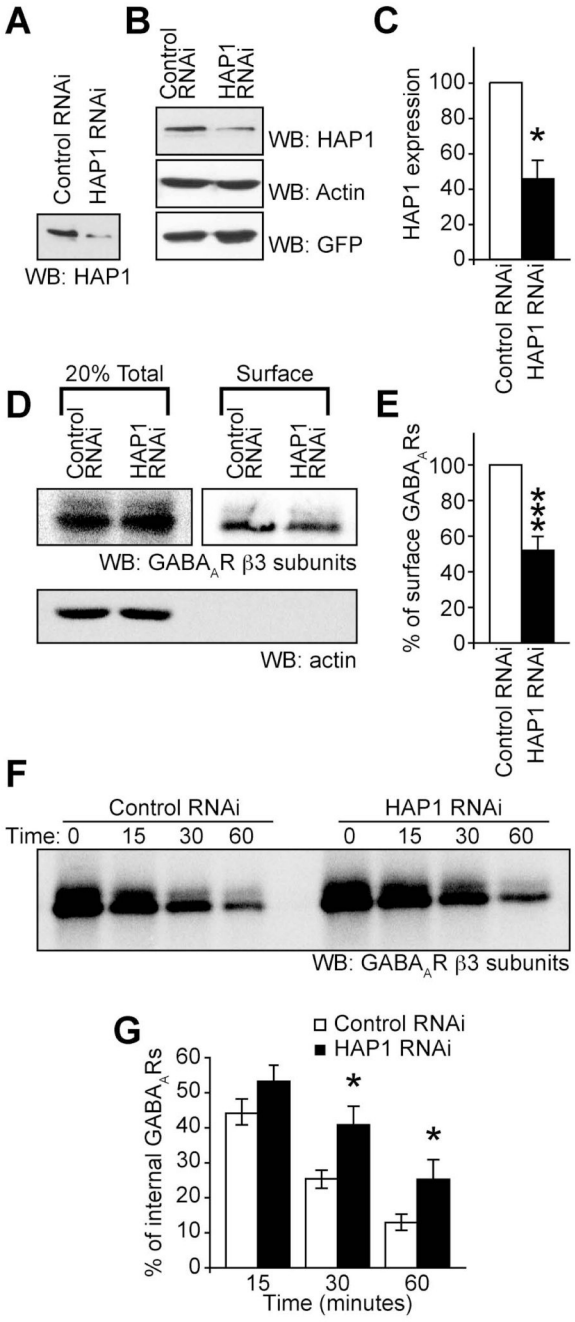

Figure 5. HAP1 knockdown disrupts surface targeting of GABA$_A$Rs

(A–C) Western blots showing knockdown with HAP1 RNAi compared to a scrambled control RNAi of exogenous HAP1 expressed in HEK cells (A) or endogenous HAP1 in neurons (B). (C) Summary bar graph of knock down in neurons with HAP1 expression normalised to actin. Error bars, s.e.m.; n = 3; $P < 0.05$, Students *t*-test.

(D, E) Expression of HAP1 RNAi reduces surface expression of GABA$_A$Rs in neurons as revealed by surface biotinylation and western blotting with anti GABA$_A$R-β3 subunit antibodies (n = 6 experiments; error bars, s.e.m.; *** $P < 0.0005$, Students *t*-test). Actin blot (D, lower panel) shows actin present in total lysates of cells, but exclusion from the surface only purified fraction of protein. (F, G) Expression of HAP1 RNAi reduces re-insertion of

internalized $GABA_A$Rs. (n = 9; Error bars, s.e.m.; *, P < 0.05, Students t-test). (F) A representative western blot of the re-insertion time course. (G) Expression of ^{GFP}KIF5B-HBD causes a reduced rate of re-insertion shown by increased levels of internal receptors at 30 and 60 minute time points. Error bars, s.e.m.; n = 7–9; * *P* < 0.05, Students *t*-test.

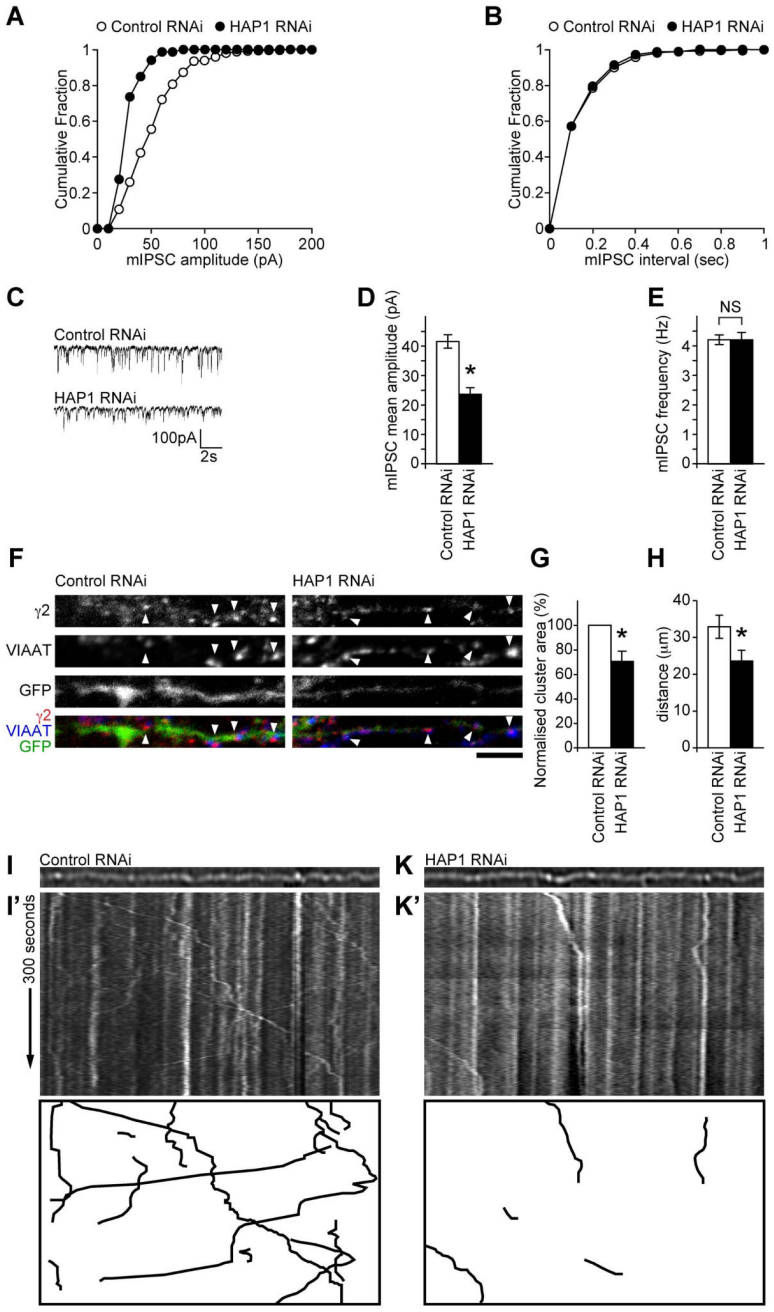

Figure 6. HAP1 knockdown disrupts synaptic targeting and trafficking of $GABA_ARs$

(A–E) Whole-cell recordings of mIPSCs from neurons transfected with HAP1 RNAi or scrambled RNAi control. (C) Representative traces demonstrating reduction in mIPSC sizes in cells transfected with HAP1 RNAi, compared to scrambled control transfected cells. Cumulative distribution plots show the mIPSC amplitude shifts to smaller amplitudes in neurons transfected with HAP1 RNAi (A), whilst there is no change in mIPSC interval (B). Summary bar graphs (D, E) show the average (mean ± s.e.m.) mIPSC amplitude and frequency of transfected neurons (Control RNAi, n = 7; HAP1 RNAi, n = 8; *, $P < 0.05$).

(F,G) $GABA_AR$ cluster analysis reveals that neurons expressing HAP1 RNAi show reduction in synaptic γ2 clusters (arrowheads) compared to scrambled control expressing cells (scale bar = 5 μm). Error bars, s.e.m.; n = 3 experiments, 24–25 neurons; *, $P < 0.05$, (Students *t*-test). (H–K') The trafficking of $\gamma2^{GFP}$-$GABA_AR$ vesicles in neurons co-expressing either control RNAi or HAP1 RNAi were analysed by video microscopy. (H) Distance travelled ± s.e.m (μm) by $\gamma2^{GFP}$-$GABA_AR$ vesicles was reduced in neurons expressing the HAP1 RNAi compared to controls (n = 45 tracks each over 4 independent experiments and 9–14 cells; *, $P < 0.05$, Students *t*-test). (I–K') Static images and kymographs showing $GABA_AR$ vesicle movement through dendrites transfected with $^{GFP}GABA_ARs$ and either control (I, I') or HAP1 RNAi (K, K'). Bottom panels show masks of kymographs to allow visualisation of only the moving vesicles.

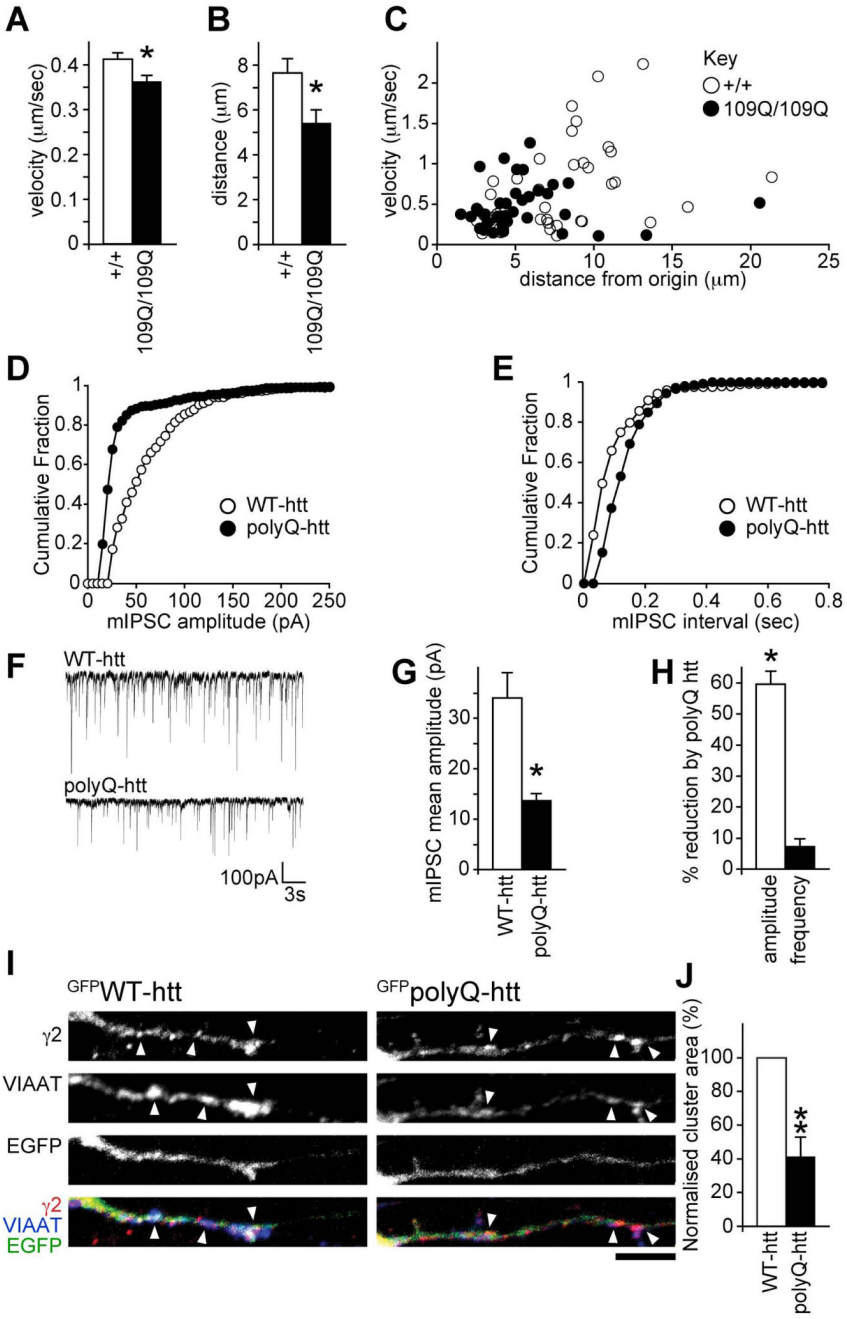

Figure 7. PolyQ-htt disrupts $GABA_AR$ trafficking and reduces synaptic inhibition

(A–C) WT (+/+) or 109Q/109Q neuronal cells expressing α1,β3 and ^{GFP}γ2 subunits were used to analyse the trafficking of $^{GFP}GABA_AR$ vesicles in real time by video microscopy. (A) Average velocity±s.e.m (μm/sec) of moving vesicles was reduced in 109Q/109Q cells compared to +/+ controls (2001 and 2082 measures respectively, 3 independent experiments). (B) The mean total distance ± s.e.m (μm) each vesicle has moved from its origin is longer in +/+ cells compared to 109Q/109Q cells (40 and 38 tracks respectively, 3 independent experiments) demonstrating a decreased processivity in mutant 109Q cells. (C) The distance from origin vs. the average velocity of each vesicle track was plotted. The main population

of $^{GFP}GABA_AR$ vesicles in 109Q/109Q cells move more slowly and for shorter distances compared to control WT (+/+) cells.

(D–H) Whole-cell recordings of mIPSCs from neurons transfected with either ^{GFP}polyQ-htt or ^{GFP}WT-htt control. Cumulative distribution plots show the mIPSC amplitude shifts to lower amplitudes in ^{GFP}polyQ-htt transfected neurons, compared to ^{GFP}WT-htt control (D), whilst there is no change in mIPSC frequency (E). Representative traces (F) demonstrating reduction in mIPSC sizes in cells transfected with ^{GFP}polyQ-htt, compared to ^{GFP}WT-htt transfected cells. Summary bar graphs (G,H) show the average (mean ± s.e.m.) mIPSC amplitude in neurons transfected with ^{GFP}WT-htt or ^{GFP}polyQ-htt, and the percentage (mean ± s.e.m.) reduction in mIPSC amplitude and interval by polyQ-htt compared to WT-htt (n = 6; * $P < 0.05$).

(I,J) $GABA_AR$ cluster analysis in neurons expressing ^{GFP}WT-htt or ^{GFP}polyQ-htt constructs reveals a reduction in synaptic γ2 clusters (arrowheads) in ^{GFP}polyQ-htt transfected neurons compared to ^{GFP}WT-htt control (scale bar = 5μm). Error bars, s.e.m.; n = 5 experiments, 19–20 neurons; **: $P < 0.01$, (Students *t*-test).